

FREQ-DP NET: A DUAL-BRANCH NETWORK FOR FENCE REMOVAL USING DUAL-PIXEL AND FOURIER PRIORS

Kunal Swami*, Sudha Velusamy*, Chandra Sekhar Seelamantula†

* Visual Intelligence Team, Samsung Research India Bangalore

† Department of Electrical Engineering, Indian Institute of Science

ABSTRACT

Removing fence occlusions from single images is a challenging task that degrades visual quality and limits downstream computer vision applications. Existing methods often fail on static scenes or require motion cues from multiple frames. To overcome these limitations, we introduce the first framework to leverage dual-pixel (DP) sensors for this problem. We propose Freq-DP Net, a novel dual-branch network that fuses two complementary priors: a geometric prior from defocus disparity, modeled using an explicit cost volume, and a structural prior of the fence’s global pattern, learned via Fast Fourier Convolution (FFC). An attention mechanism intelligently merges these cues for highly accurate fence segmentation. To validate our approach, we build and release a diverse benchmark with different fence varieties. Experiments demonstrate that our method significantly outperforms strong general-purpose baselines, establishing a new state-of-the-art for single-image, DP-based fence removal.

Index Terms— obstruction removal, fence removal, dual-pixel sensor, diverse fence removal dataset

1. INTRODUCTION

In an era where computer vision systems demand clear visual data, real-world scenes are frequently compromised by foreground obstructions. Among the most pervasive are fences, whose diverse structures, varying in material, thickness, and pattern density, pose a formidable challenge. These occlusions create a critical failure point for automated systems, catastrophically degrading the performance of object detectors [1], segmentation models, and trackers essential for autonomous driving [2] and robotics [3]. Effectively “seeing through” these varied fences from a single image is thus a crucial step towards robust machine perception.

Existing solutions for this problem face significant limitations. Methods that rely on motion parallax from multi-frame captures [4, 5] are often impractical for the user and fail entirely in static scenes, while single-image approaches struggle with the inherent ambiguity between the fence and background. Furthermore, the development of truly generalizable solutions has been hampered by a narrow focus on limited, non-diverse datasets [5], leading to methods that overfit

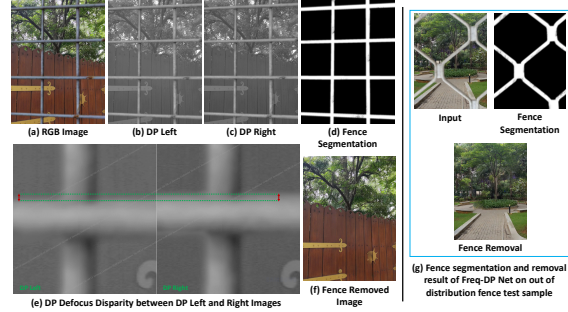


Fig. 1: From a single input (a), we leverage disparity between the left (b) and right (c) DP views to generate a precise mask (d), which guides a model to produce the final result (f). Zoomed-in patches (e) highlight the disparity cue. DP views are grayscale (from the sensor’s green channel). We use ‘left/right’ terminology for consistency, the smartphone disparity is typically vertical. (g) shows our result on an out-of-distribution fence sample. Please zoom in for better detail.

to specific patterns. To overcome these challenges, we introduce the first framework to leverage the rich physical information from a dual-pixel (DP) sensor [6, 7]. Our approach is built on fusing two complementary cues: geometric information derived from the fence’s defocus disparity, which relies on the practical assumption that the background is in focus, and the fence’s global structural patterns captured in the frequency domain. This fusion of appearance-invariant priors allows us to achieve a new state-of-the-art in fence removal, as demonstrated in our teaser (Fig. 1), enabling more robust visual understanding.

Following are the **major contributions** of our method:

- The first framework for single-image fence removal using appearance-invariant disparity cues from a DP sensor.
- Freq-DP Net, a novel dual-branch network that fuses geometric cues from a DP cost volume with global structural patterns learned via Fast Fourier Convolutions (FFCs).
- We build and release the most diverse benchmark for this task, featuring varied fences and a test set of 150 real-world (RGB-DP-GT) and 100 synthetic (RGB-DP-GT-Mask) scenes.
- A new state-of-the-art on our benchmark, significantly outperforming strong general-purpose baselines.

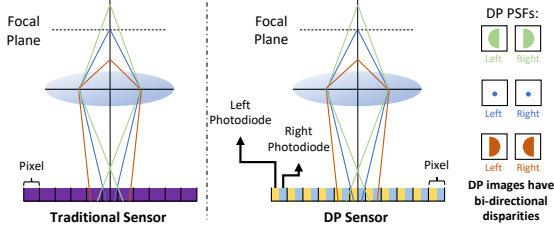


Fig. 2: DP sensor image formation.

2. RELATED WORK

2.1. DP Sensor

A dual-pixel (DP) sensor captures two perspectives of a scene in a single shot by splitting each pixel into left and right photodiodes (Fig. 2). While in-focus points are imaged identically, out-of-focus points project to different locations, creating a shift between the left-view (I_L) and right-view (I_R) known as defocus disparity. The disparity's direction depends on whether a point is in front of or behind the focal plane, and its magnitude is proportional to the point's distance from it. This relationship can be modeled by convolving a latent sharp image I_{sharp} with distinct, depth-dependent Point Spread Functions (PSFs) for each view (k_d^L, k_d^R) [7, 8]:

$$I_v = I_{sharp} \circledast k_d^v, \quad v \in \{L, R\} \quad (1)$$

where the combined image $I_C = (I_L + I_R)/2$ is blurred by an effective PSF $k_d^C = (k_d^L + k_d^R)/2$. This defocus disparity provides a powerful, appearance-invariant cue for occlusion analysis. Note that smartphones limit DP photodiodes to the green pixels, producing grayscale DP views.

2.2. Fence Removal

Prior works on obstruction removal often model the scene as a composite of two layers [9, 10], typically leveraging motion parallax from video to distinguish them. This reliance on multi-frame captures is problematic as it is often impractical for the user, fails for static scenes, and in some cases, requires a pre-existing fence mask for removal [9, 10].

Fence-specific literature has similarly evolved from classical methods [11, 12] to deep learning approaches that depend on multi-frame bursts [4], video [5], or multiple cameras [13]. Progress in this area has been critically bottlenecked by the reliance on a single, non-diverse public dataset [5], which contains only one type of metallic, diamond-patterned fence, leading to methods that overfit to a simple pattern and its appearance [4]. While recent efforts like Instruct2See [14] have begun addressing these cross-distribution challenges by learning to remove varied obstructions, significant gaps remain: (i) the lack of a diverse benchmark for robust evaluation, and (ii) an over-reliance on motion or appearance cues, creating a need for a single-image method that uses a more robust physical prior.

3. DATASET GENERATION

A core contribution of this work is the establishment of the first comprehensive framework for DP based fence removal,



Fig. 3: Our dataset features a wide range of fence structures, varying in pattern, material, and thickness.

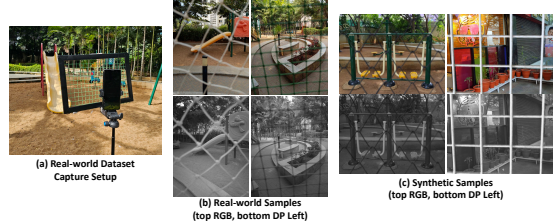


Fig. 4: Real-world dataset capture setup, and real-world and synthetic dataset samples. Please zoom in for better detail. necessitated by the absence of public data for this task. We introduce two key components: (i) a synthetic data pipeline for generating a large-scale training set, and (ii) a public benchmark for evaluation. Unlike existing works that are limited to a single fence type [5], our benchmark consists of both synthetic and captured real-world test scenes featuring a wide variety of fence structures (see Fig. 3). This enables, for the first time, standardized training and rigorous comparison of methods on this challenging problem.

3.1. Real-World Dataset Collection

To create a benchmark for real-world evaluation, we captured 150 paired scenes. Using a tripod-mounted Google Pixel 4 with its focus set on the background, we recorded a clean scene, followed by an occluded version using custom-built fence frames. To ensure diversity, these frames featured the various physical fences (some are shown in Fig. 3) which were placed at varying distances from the camera to produce a range of defocus effects. Raw DP views were extracted using a custom application based on [15, 16]. Finally, to ensure pair quality, all images were manually checked for major misalignments and normalized for lighting via histogram matching. Our capture setup and samples are detailed in Fig. 4.

3.2. Synthetic Dataset Generation

To enable robust, physics based training, our synthesis pipeline composites new, all-in-focus fence assets onto real, clean DP and RGB backgrounds. This hybrid approach preserves the sensor's authentic optical properties (e.g., lens vignetting, sensor noise). As existing datasets [5] lack diversity and provide pre-blurred fences unsuitable for our renderer, we captured and manually segmented various all-in-focus fences, some visual examples of which are shown in Fig. 3. To further increase diversity, we augment these assets before compositing: geometric augmentations are applied to both the fence texture F and its mask M for alignment, while color augmentations are applied only to the texture F .

Algorithm 1 DP and RGB Fence Synthesis Pipeline

```

1: Input: Clean views ( $I_L, I_R, I_C$ ), Fence RGB texture
    $F_{rgb}$ , Mask  $M$ , PSF grids ( $K_L, K_R$ ).
2: Output: Occluded views ( $I'_L, I'_R, I'_C$ ).
3:  $K_C \leftarrow (K_L + K_R)/2$ 
4:  $d \sim U(10\text{cm}, 50\text{cm})$ ;  $\alpha \propto 1/d$ 
5:  $K_v^\alpha \leftarrow \text{scale}(K_v, \alpha)$  for  $v \in \{L, R, C\}$ .
6: Apply identical geometric augmentations to  $F_{rgb}, M$ .
7: Apply color augmentations only to fence texture  $F_{rgb}$ .
8:  $F \leftarrow F_{rgb}$ 's green channel {Use green channel for DP}
9: for  $v$  in  $\{L, R, C\}$  do
10:   if  $v = C$  then
11:     Process each channel  $I_{C,c}$  with  $F_{rgb,c}$  independently.
12:   else
13:     Process single-channel view  $I_v$  with grayscale fence
         $F$ .
14:   end if
15:    $I_{v,sharp} \leftarrow I_v \odot (1 - M) + F \odot M$ .
16:    $I_{v,blur} \leftarrow \text{PatchwiseConv}(I_{v,sharp}, K_v^\alpha)$ .
17:    $M_{v,blur} \leftarrow \text{PatchwiseConv}(M, K_v^\alpha)$ .
18:    $I'_v \leftarrow I_v \odot (1 - M_{v,blur}) + I_{v,blur} \odot M_{v,blur}$ .
19: end for
20: return ( $I'_L, I'_R, I'_C$ ).

```

Our simulation leverages the spatially-varying PSFs calibrated by [17], which require a patch-wise application. To simulate varying fence distances, we randomly sample a fence depth d and calculate the corresponding blur scale α based on the thin lens model ($\alpha \propto |\frac{1}{d_{focus}} - \frac{1}{d}|$, where d_{focus} is the focus distance) [18]. To model a camera focused on a distant background, we assume an infinite focus distance, which simplifies the relationship to $\alpha \propto 1/d$. The full synthesis pipeline, which involves compositing an augmented fence onto the clean views, blurring both the composite and mask, and then performing a final blend, is detailed in Alg. 1. This process is applied to the DP views and to each channel of the RGB view independently. The final dataset consists of 904 synthetic samples (804 train, 100 test). Following [8], from the high-resolution (2016×1536) training samples, we extract $\approx 13.7k$ patches of size 512×512 for training.

4. PROPOSED METHOD

4.1. Freq-DP Net

To accurately segment the fence, we propose Freq-DP Net, a dual-branch encoder-decoder network that fuses geometric cues with structural frequency-domain priors. The overall architecture is shown in Fig. 5.

4.1.1. DP Disparity Branch

This branch takes the DP views (I_L, I_R) as input. A shared-weight 2D feature extractor based on residual blocks first produces feature maps $F_L, F_R \in \mathbb{R}^{C' \times H/2 \times W/2}$. We then con-

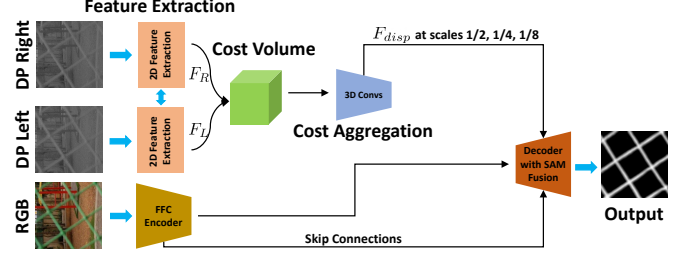


Fig. 5: Network architecture of Freq-DP Net.

struct a 3D cost volume [19] by correlating these features at sub-pixel precision:

$$C(\mathbf{p}, d) = \langle F_L(\mathbf{p}), \phi(F_R, \mathbf{p} - \mathbf{d}) \rangle \quad (2)$$

where $\mathbf{p} = (x, y)$ is a pixel coordinate, $\mathbf{d} = (d, 0)$, $\langle \cdot, \cdot \rangle$ is the inner product, and ϕ is the phase-shift interpolation [20] function. Since the fence lies on one side of the focal plane, the DP disparity is unidirectional [7], defining our search range as $d \in [0, D_{max}]$. This volume is processed by a series of 3D convolutions to produce disparity features (F_{disp}) at scales $H/2 \times W/2$, $H/4 \times W/4$, and $H/8 \times W/8$.

4.1.2. Structural Frequency Branch & Fusion

The structural branch is a symmetric, U-Net [21] like encoder-decoder built with FFC convolution layers [22] that processes the composite (RGB) image I_C . To leverage both cues, the disparity features F_{disp} from the DP branch are fused into the FFC decoder. This fusion is performed selectively by a Structural Attention Module (SAM) only at the stages where disparity features are available ($H/2 \times W/2$, $H/4 \times W/4$, and $H/8 \times W/8$). At these stages, F_{disp} modulates the FFC decoder's features F'_{ffc} :

$$F'_{ffc} = F_{ffc} \odot \sigma(\text{Conv}_{1 \times 1}(F_{disp})) \quad (3)$$

where F'_{ffc} are the refined features passed to the next decoder block. This guides the decoder to focus on regions that exhibit both a strong disparity signal and a fence-like structure. At other scales, the FFC decoder relies solely on its own skip connections. The final layer of the FFC decoder produces the soft segmentation mask.

4.2. Fence Removal

For the final restoration, the predicted mask and RGB image are fed to LaMa-Fence, our version of the LaMa [23] inpainting network finetuned on our synthetic data to handle thin, repetitive fence patterns.

5. RESULTS AND DISCUSSION

We train Freq-DP Net on our synthetic dataset of size $\approx 13.7k$ and evaluate it on two test sets: 150 real-world scenes and a held-out synthetic set of 100 scenes, which also include unseen fence types to test for generalization. We assess performance on both the primary task of fence segmentation and the final application of fence removal.

Table 1: Quantitative comparison for fence segmentation.

Method	Precision	Recall	F1
RGB UNet	0.776	0.753	0.764
DP UNet	0.936	0.921	0.928
Freq-DP Net	0.979	0.964	0.971

Table 2: Quantitative comparison for end-to-end fence removal on our synthetic and real test sets.

Method	Synthetic Test Set		Real Test Set	
	PSNR \uparrow	SSIM \uparrow	PSNR \uparrow	SSIM \uparrow
Restormer (RGB)	32.23	0.9457	29.78	0.8875
LaMa (RGB)	30.67	0.9323	28.45	0.8763
Restormer (RGB+DP)	39.89	0.9754	31.54	0.9012
LaMa (RGB+DP)	37.72	0.9623	30.67	0.8932
Ours (Freq-DP Net + LaMa-Fence)	41.28	0.9876	34.54	0.9223

5.1. Fence Segmentation

We evaluate our core contribution of fence segmentation against baselines with a similar parameter count for a fair comparison. As shown in Tab. 1, our Freq-DP Net significantly outperforms both RGB U-Net and DP U-Net (RGB+DP concatenated input). The inferior performance of the RGB U-Net confirms that a single RGB modality is insufficient for this diverse task. Freq-DP Net’s success is mirrored in the qualitative results in Fig. 6, where our method produces cleaner masks and demonstrates superior generalization to challenging, out-of-distribution fence types (e.g., the third row). This validates our physics-based, dual-branch design, which is more robust than appearance-based models.

5.2. Fence Removal

Next, we evaluate the final restoration quality. We compare our two-stage pipeline against powerful end-to-end baselines: Restormer [24] and LaMa [23]. We test two variants for each baseline: an RGB-only version, and an RGB+DP version that takes a 5-channel input from the concatenated RGB and DP images. Tab. 2 shows our method achieves higher PSNR and SSIM scores on both synthetic and real-world test sets. The strong performance on the real-world set is particularly important, as it demonstrates our model’s effective generalization from synthetic training data. Visual comparisons in Fig. 7 also show that our approach performs more accurate restoration with fewer artifacts. Note that we only visualize the stronger performing RGB+DP variants of the baselines.

5.3. Ablation Study

Finally, our ablation study in Tab. 3 quantitatively validates our architectural choices. All ablation variants use same parameters as our full model ($\approx 22.4M$) to control for model capacity. The results clearly demonstrate the contribution of each component. Removing either the DP cost volume or the FFC encoder significantly degrades segmentation performance, confirming that explicitly modeling both geometric disparity and global structure are crucial. Furthermore, we test a variant where our SAM Fusion is replaced with simple feature concatenation. This also reduces performance, proving that the intelligent fusion via SAM is more effective than a naïve merge, and that all proposed components work synergistically to achieve the final result.

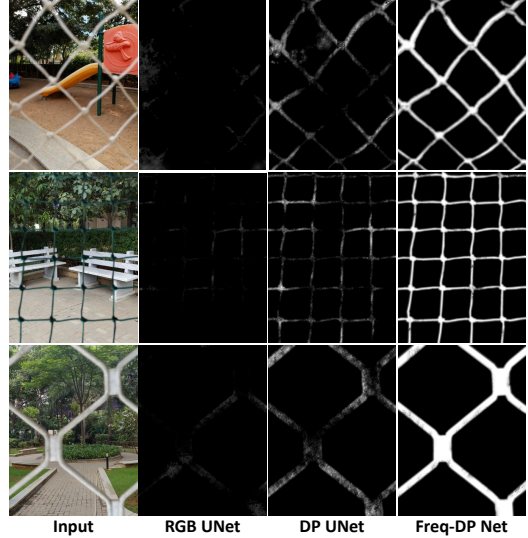


Fig. 6: Qualitative results for fence segmentation. The third row highlights our model’s successful generalization to a fence type unseen during training.



Fig. 7: Qualitative results for fence removal.

Table 3: Ablation study for fence segmentation.

Ablation Setting	Precision	Recall	F1
No Cost Volume (in short, CV)	0.943	0.931	0.937
No FFC based Encoder (in short, FFC)	0.958	0.947	0.952
No CV and FFC (same as DP UNet)	0.936	0.921	0.928
No SAM Fusion	0.968	0.955	0.961
Freq-DP Net	0.979	0.964	0.971

6. CONCLUSION AND FUTURE WORK

We introduced the first framework leveraging dual-pixel (DP) sensors for single-image fence removal. Our network, Freq-DP Net, establishes a new state-of-the-art on our newly released diverse benchmark. Despite its performance, our method has limitations: DP cues weaken as fence distance increases, and the single-image formulation requires generative inpainting for occluded regions, whereas video-based methods can retrieve pixels from adjacent frames for more faithful results. Nevertheless, this work demonstrates the power of physics-based sensor cues for complex occlusions. Future work will handle multiple occlusion types in a unified model.

7. REFERENCES

- [1] Angtian Wang, Yihong Sun, Adam Kortylewski, and Alan L Yuille, “Robust object detection under occlusion with context-aware compositionalnets,” in *CVPR*, 2020, pp. 12645–12654.
- [2] Shane Gilroy, Edward Jones, and Martin Glavin, “Overcoming occlusion in the automotive environment—a review,” *IEEE Transactions on Intelligent Transportation Systems*, vol. 22, no. 1, pp. 23–35, 2019.
- [3] Mengdi Li, Cornelius Weber, Matthias Kerzel, Jae Hee Lee, Zheni Zeng, Zhiyuan Liu, and Stefan Wermter, “Robotic occlusion reasoning for efficient object existence prediction,” in *IROS*, 2021, pp. 2686–2692.
- [4] Stavros Tsogkas, Fengjia Zhang, Allan D. Jepson, and Alex Levinshtein, “Efficient flow-guided multi-frame de-fencing,” in *WACV*, 2023, pp. 1838–1847.
- [5] Chen Du, Byeongkeun Kang, Zheng Xu, Ji Dai, and Truong Q. Nguyen, “Accurate and efficient video de-fencing using convolutional neural networks and temporal information,” in *ICME*, 2018, pp. 1–6.
- [6] Liyuan Pan, Shah Chowdhury, Richard Hartley, Miao-miao Liu, Hongguang Zhang, and Hongdong Li, “Dual pixel exploration: Simultaneous depth estimation and image restoration,” in *CVPR*, 2021, pp. 4340–4349.
- [7] Feiran Li, Heng Guo, Hiroaki Santo, Fumio Okura, and Yasuyuki Matsushita, “Learning to synthesize photorealistic dual-pixel images from RGBD frames,” in *ICCP*, 2023, pp. 1–11.
- [8] Abdullah Abuolaim and Michael S. Brown, “Defocus deblurring using dual-pixel data,” in *ECCV*, 2020, pp. 111–126.
- [9] Tianfan Xue, Michael Rubinstein, Ce Liu, and William T. Freeman, “A computational approach for obstruction-free photography,” *ACM Trans. Graph.*, vol. 34, no. 4, pp. 79:1–79:11, 2015.
- [10] Yu-Lun Liu, Wei-Sheng Lai, Ming-Hsuan Yang, Yung-Yu Chuang, and Jia-Bin Huang, “Learning to see through obstructions with layered decomposition,” *IEEE Trans. Pattern Anal. Mach. Intell.*, vol. 44, no. 11, pp. 8387–8402, 2022.
- [11] Yanxi Liu, Tamara Belkina, James Hays, and Roberto Lublinerman, “Image de-fencing,” in *CVPR*, 2008.
- [12] Minwoo Park, Kyle Brocklehurst, Robert T. Collins, and Yanxi Liu, “Image de-fencing revisited,” in *ACCV*, 2010, vol. 6495, pp. 422–434.
- [13] Sankaraganesh Jonna, Sukla Satapathy, and Rajiv R. Saray, “Stereo image de-fencing using smartphones,” in *ICASSP*, 2017, pp. 1792–1796.
- [14] Junhang Li, Yu Guo, Chuhua Xian, and Shengfeng He, “Instruct2see: Learning to remove any obstructions across distributions,” in *ICML*, 2025.
- [15] Rahul Garg, Neal Wadhwa, Sameer Ansari, and Jonathan T. Barron, “Learning single camera depth estimation using dual-pixels,” in *ICCV*, 2019, pp. 7627–7636.
- [16] “Android app to capture dual-pixel data,” https://github.com/google-research/google-research/blob/master/dual_pixels/README.md#android-app-to-capture-dual-pixel-data, Accessed: September 02, 2025.
- [17] Shumian Xin, Neal Wadhwa, Tianfan Xue, Jonathan T. Barron, Pratul P. Srinivasan, Jiawen Chen, Ioannis Gkioulekas, and Rahul Garg, “Defocus map estimation and deblurring from a single dual-pixel image,” in *ICCV*, 2021, pp. 2208–2218.
- [18] Richard Hartley and Andrew Zisserman, *Multiple View Geometry in Computer Vision*, Cambridge University Press, 2nd edition, 2003.
- [19] Jia-Ren Chang and Yong-Sheng Chen, “Pyramid stereo matching network,” in *CVPR*, 2018, pp. 5410–5418.
- [20] Hae-Gon Jeon, Jaesik Park, Gyeongmin Choe, Jinsun Park, Yunsu Bok, Yu-Wing Tai, and In So Kweon, “Accurate depth map estimation from a lenslet light field camera,” in *CVPR*, 2015, pp. 1547–1555.
- [21] Olaf Ronneberger, Philipp Fischer, and Thomas Brox, “U-net: Convolutional networks for biomedical image segmentation,” in *MICCAI*, 2015, pp. 234–241.
- [22] Lu Chi, Borui Jiang, and Yadong Mu, “Fast fourier convolution,” in *NeurIPS*, 2020, vol. 33, pp. 1053–1064.
- [23] Roman Suvorov, Elizaveta Logacheva, Anton Mashikhin, Anastasia Remizova, Arsenii Ashukha, Aleksei Silvestrov, Naejin Kong, Harshith Goka, Ki-woong Park, and Victor Lempitsky, “Resolution-robust large mask inpainting with fourier convolutions,” in *WACV*, 2022, pp. 3172–3182.
- [24] Syed Waqas Zamir, Aditya Arora, Salman Khan, Munawar Hayat, Fahad Shahbaz Khan, and Ming-Hsuan Yang, “Restormer: Efficient transformer for high-resolution image restoration,” in *CVPR*, 2022, pp. 5718–5729.